20

Signal Calibration, Estimation for Real-Time Monitoring and Control[‡]

Asok Ray and Shashi Phoha

20.1 Introduction

Performance, reliability, and safety of complex dynamical processes such as aircraft and power plants depend upon validity and accuracy of sensor signals that measure plant conditions for information display, health monitoring, and control [1]. Redundant sensors are often installed to generate spatially averaged time-dependent estimates of critical variables so that reliable monitoring and control of the plant are assured. Examples of redundant sensor installations in complex engineering applications are:

- Inertial navigational sensors in both tactical and transport aircraft for guidance and control [2,3].
- Neutron flux detectors in the core of a nuclear reactor for fuel management, health monitoring, and power control [4].
- Temperature, pressure, and flow sensors in both fossil-fuel and nuclear steam power plants for health monitoring and feedforward–feedback control [5].

Sensor redundancy is often augmented with analytical measurements that are obtained from physical characteristics and/or model of the plant dynamics in combination with other available sensor data [4,6]. The redundant sensors and analytical measurements are referred to as redundant measurements in the following.

Individual measurements in a redundant set may often exhibit deviations from each other after a length of time. These differences could be caused by slowly time-varying sensor parameters (e.g. amplifier gain), plant parameters (e.g. structural stiffness and heat transfer coefficient), transport delays, etc. Consequently, some of the redundant measurements could be deleted by a fault detection and

[‡]The research work reported in this chapter has been supported in part by the Army Research Office under Grant No. DAAD19-01-1-0646.

0-8493-XXXX-X/04/$0.00+$1.50

isolation (FDI) algorithm [7] if they are not calibrated periodically. On the other hand, failure to isolate a degraded measurement could cause an inaccurate estimate of the measured variable by, for example, increasing the threshold bound in the FDI algorithm. In this case, the plant performance may be adversely affected if that estimate is used as an input to the decision and control system. This problem can be resolved by adaptively filtering the set of redundant measurements as follows:

- All measurements, which are consistent relative to the threshold of the FDI algorithm, are simultaneously calibrated on-line to compensate for their relative errors.
- The weights of individual measurements for computation of the estimate are adaptively updated on-line based on their respective *a posteriori* probabilities of failure instead of being fixed *a priori*.

In the event of an abrupt disruption of a redundant measurement in excess of its allowable bound, the respective measurement is isolated by the FDI logic, and only the remaining measurements are calibrated to provide an unbiased estimate of the measured variable. On the other hand, if a gradual degradation (e.g. a sensor drift) occurs, the faulty measurement is not immediately isolated by the FDI logic. However, its influence on the estimate and calibration of the remaining measurements is diminished as a function of the magnitude of its residual (i.e. deviation from the estimate), which is an indicator of its degradation. This is achieved by decreasing the relative weight of the degraded measurement as a monotonic function of its deviation from the remaining measurements. Thus, if the error bounds of the FDI algorithm are appropriately increased to reduce the probability of false alarms, then the resulting delay in detecting a gradual degradation could be tolerated. The rationale is that an undetected fault, as a result of the adaptively reduced weight, would have smaller bearing on the accuracy of measurement calibration and estimation. Furthermore, since the weight of a gradually degrading measurement is smoothly reduced, the eventual isolation of the fault would not cause any abrupt change in the estimate. This feature, known as *bumpless* transfer in the process control literature, is very desirable for plant operation.

This chapter presents a calibration and estimation filter for redundancy management of sensor data and analytical measurements. The filter is validated based on redundant sensor data of throttle steam temperature collected from an operating power plant. Development and validation of the filter algorithm are presented in the main body of the chapter along with concluding remarks. Appendix A presents the theory of multiple hypotheses based on the *a posteriori* probability of failure of a single measurement [8].

AQ1

20.2 Signal Calibration and Measurement Estimation

A redundant set of ℓ sensors and/or analytical measurements of an n-dimensional plant variable are modeled at the kth sample as

$$m_k = (H + \Delta H_k)x_k + b_k + e_k \tag{20.1}$$

where m_k is the $(\ell \times 1)$ vector of (uncalibrated) redundant measurements; H is the $(\ell \times n)$ *a priori* determined matrix of scale factor having rank n, with $\ell > n \geq 1$; ΔH_k is the $(\ell \times n)$ matrix of scale factor errors; x_k is the $(n \times 1)$ vector of true (unknown) value of the measured variable; b_k is the $(\ell \times 1)$ vector of bias errors; and e_k is the $(\ell \times 1)$ vector of measurement noise, such that $E[e_k] = 0$ and $E[e_k e_l^{\mathrm{T}}] = R_k \delta_{kl}$.

The noise covariance matrix R_k of uncalibrated measurements plays an important role in the adaptive filter for both signal calibration and measurement estimation. It is shown in the following how R_k is recursively tuned based on the history of calibrated measurements.

Equation (20.1) is rewritten in a more compact form as

$$m_k = Hx_k + c_k + e_k \tag{20.2}$$

where the correction c_k due to the combined effect of bias and scale-factor errors is defined as

$$c_k \equiv \Delta H_k x_k + b_k \tag{20.3}$$

The objective is to obtain an unbiased predictor estimate $\hat{c}_k$ of the correction c_k so that the sensor output m_k can be calibrated at each sample. A recursive relation of the correction c_k is modeled similar to a random walk process as

$$\begin{aligned} c_{k+1} &= c_k + v_k \\ E[v_k] &= 0; \quad E[v_k v_j] = Q\delta_{kj} \text{ and } E[v_k e_j] = 0 \quad \forall k, j \end{aligned} \tag{20.4}$$

where the stationary noise v_k represents uncertainties of the model in Equation (20.4).

We construct a filter to calibrate each measurement with respect to the remaining redundant measurements. The filter input is the parity vector p_k of the uncalibrated measurement vector m_k, which is defined [2,9] as

$$p_k = Vm_k \tag{20.5}$$

where the rows of the projection matrix $V \in \Re^{(\ell-n)\times\ell}$ form an orthonormal basis of the left null space of the measurement matrix $H \in \Re^{\ell\times n}$ in Equation (20.1), i.e.

$$\begin{aligned} VH &= 0_{(\ell-n)\times n} \\ VV^{\mathrm{T}} &= I_{(\ell-n)\times(\ell-n)} \end{aligned} \tag{20.6}$$

and the columns of V span the parity space that contains the parity vector. A combination of Equations (20.2), (20.4), (20.5) and (20.6) yields

$$p_k = Vc_k + \varepsilon_k \tag{20.7}$$

where the noise $\varepsilon_k \equiv Ve_k$ having $E[\varepsilon_k] = 0$ and $E[\varepsilon_k \varepsilon_j^{\mathrm{T}}] \equiv VR_kV^{\mathrm{T}}\delta_{kj}$. If the scale-factor error matrix ΔH_k belongs to the column space of H, then the parity vector p_k is independent of the true value x_k of the measured variable. Therefore, for $\|V\Delta H_k x_k\| \ll \|Vb_k\|$, which includes relatively small scale-factor errors, the calibration filter operates approximately independent of x_k.

Now we proceed to construct a recursive algorithm to predict the estimated correction $\hat{c}_k$ based on the principle of best linear least-squares estimation that has the structure of an optimal minimum-variance filter [10,11] and uses Equations (20.4) and (20.7):

$$\left.\begin{aligned} \hat{c}_{k+1} &= \hat{c}_k + K_k\gamma_k && \text{given } \hat{c}_0 \\ P_{k+1} &= (I - K_kV)P_k + Q && \text{given } P_0 \text{ and } Q \\ K_k &= P_kV^{\mathrm{T}}\left(V[R_k + P_k]V^{\mathrm{T}}\right)^{-1} && \text{given } R_k \\ \gamma_k &= p_k - V\hat{c}_k && \text{innovation} \end{aligned}\right\} \tag{20.8}$$

Upon evaluation of the unbiased estimated correction $\hat{c}_k$, the uncalibrated measurement m_k is compensated to yield the calibrated measurement y_k as

$$y_k = m_k - \hat{c}_k \tag{20.9}$$

Using Equations (20.5) and (20.9), the innovation γ_k in Equation (20.8) can be expressed as the projection of the calibrated measurement y_k onto the parity space, i.e.

$$\gamma_k = V y_k \tag{20.10}$$

By setting $\Gamma_k \equiv K_k V$, we obtain an alternative form of the recursive relations in Equation (20.8) as

$$\begin{aligned} \hat{c}_{k+1} &= \hat{c}_k + \Gamma_k y_k && \text{given } \hat{c}_0 \\ P_{k+1} &= (I - \Gamma_k) P_k + Q && \text{given } P_0 \text{ and } Q \\ \Gamma_k &= P_k V^{\mathrm{T}} \left(V[R_k + P_k] V^{\mathrm{T}} \right)^{-1} V && \text{given } R_k \end{aligned} \tag{20.11}$$

Note that the inverse of the matrix $\left(V[R_k + P_k]V^{\mathrm{T}}\right)$ in Equations (20.8) and (20.11) exists because the rows of V are linearly independent, $R_k > 0$, and $P_k \geq 0$.

Next we obtain an unbiased weighted least squares estimate $\hat{\boldsymbol{x}}_k$ of the measured variable x_k based on the calibrated measurement y_k as

$$\hat{\boldsymbol{x}}_k = (H^{\mathrm{T}} R_k^{-1} H)^{-1} H^{\mathrm{T}} R_k^{-1} y_k \tag{20.12}$$

The inverse of the (symmetric positive-definite) measurement covariance matrix R_k serves as the weighting matrix for generating the estimate $\hat{\boldsymbol{x}}_k$, and is used as a filter matrix. Compensation of a (slowly varying) undetected error in the jth measurement out of ℓ redundant measurements causes the largest jth element $\left|{}_j\hat{c}_k\right|$ in the correction vector $\hat{c}_k$. Therefore, a limit check on the magnitude of each element of $\hat{c}_k$ will allow detection and isolation of the degraded measurement. The bounds of limit check, which could be different for the individual elements of $\hat{c}_k$, are selected by trade-off between the probability of false alarms and the allowable error in the estimate $\hat{\boldsymbol{x}}_k$ of the measured variable [12].

20.2.1 Degradation Monitoring

Following Equation (20.12), we define the residual η_k of the calibrated measurement y_k as

$$\eta_k = y_k - H\hat{\boldsymbol{x}}_k \tag{20.13}$$

The residuals represent a measure of relative degradation of individual measurements. For example, under the normal condition, all calibrated measurements are clustered together, i.e. $\|\eta_k\| \approx 0$, although this may not be true for the residual $(m_k - H\hat{\boldsymbol{x}}_k)$ of uncalibrated measurements.

While large abrupt changes in excess of the error threshold are easily detected and isolated by a standard diagnostics procedure (e.g. [7]), small errors (e.g. slow drift) can be identified from the *a posteriori* probability of failure that is recursively computed from the history of residuals based on the following trinary hypotheses:

$$\begin{aligned} H^0 &: \textit{Normal behavior with} \text{ a priori } \textit{conditional density function } {}_jf^0(\cdot) \equiv {}_jf\left(\cdot \middle| H^0\right) \\ H^1 &: \textit{High (positive) failure with} \text{ a priori } \textit{conditional density function } {}_jf^1(\cdot) \equiv {}_jf\left(\cdot \middle| H^1\right) \\ H^2 &: \textit{Low (negative) failure with} \text{ a priori } \textit{conditional density function } {}_jf^2(\cdot) \equiv {}_jf\left(\cdot \middle| H^2\right) \end{aligned} \tag{20.14}$$

where the left subscript refers to of the jth measurement for $j = 1, 2, \ldots, \ell$, and the right superscript indicates the normal behavior or failure mode. The density function for each residual is determined

a priori from experimental data and/or instrument manufacturers' specifications. Only one test is needed here to accommodate both positive and negative failures; this is in contrast to the binary hypotheses, which require two tests. We now apply the recursive relations for multi-level hypotheses testing of single variables, derived in Appendix A, to each residual of the redundant measurements. Then, for the jth measurement at the kth sampling instant, *a posteriori* probability of failure ${}_j\Pi_k$ is obtained following Equation (20.A17) as

$$\left.\begin{aligned} {}_j\Psi_k &= \left(\frac{{}_jp + {}_j\Psi_{k-1}}{2(1-{}_jp)}\right)\left(\frac{{}_jf^1({}_j\eta_k) + {}_jf^2({}_j\eta_k)}{{}_jf^0({}_j\eta_k)}\right) \\ {}_j\Pi_k &= \frac{{}_j\Psi_k}{1+{}_j\Psi_k} \end{aligned}\right\} \tag{20.15}$$

where ${}_jp$ is the *a priori* probability of failure of the jth sensor during one sampling period, and the initial condition of each state, ${}_j\Psi_0, j = 1, 2, \ldots, \ell$, needs to be specified.

Based on the *a posteriori* probability of failure, we now proceed to formulate a recursive relation for the measurement noise covariance matrix R_k that influences both calibration and estimation as seen in Equations (20.8) to (20.12). Its initial value R_0, which is determined *a priori* from experimental data and/or instrument manufacturers' specifications, provides the *a priori* information on individual measurement channels and conforms to the normal operating conditions when all measurements are clustered together, i.e. $\|\eta_k\| \approx 0$. In the absence of any measurement degradation, R_k remains close to its initial value R_0. Significant changes in R_k may take place if one or more sensors start degrading. This phenomenon is captured by the following model:

$$R_k = \sqrt{R_k^{\text{rel}}}R_0\sqrt{R_k^{\text{rel}}} \quad \text{with} \quad R_0^{\text{rel}} = I \tag{20.16}$$

where R_k^{rel} is a positive-definite diagonal matrix representing relative performance of the individual calibrated measurements and is recursively generated as follows:

$$R_{k+1}^{\text{rel}} = \text{diag}\big[h({}_j\Pi_k)\big], \quad \text{i.e. } {}_jr_{k+1}^{\text{rel}} = h({}_j\Pi_k) \tag{20.17}$$

where ${}_jr_k^{\text{rel}}$ and ${}_j\Pi_k$ are respectively the relative variance and *a posteriori* probability of failure of the jth measurement at the kth instant; and h: $[0, 1) \to [1, \infty)$ is a continuous monotonically increasing function with boundary conditions $h(0) = 1$ and $h(\varphi) \to \infty$ as $\varphi \to 1$.

The implication of Equation (20.17) is that the credibility of a sensor monotonically decreases with increase in its variance, which tends to infinity as its *a posteriori* probability of failure approaches unity. The magnitude of the relative variance ${}_jr_k^{\text{rel}}$ is set to the minimum value of one for zero *a posteriori* probability of failure. In other words, the jth diagonal element ${}_jw_k^{\text{rel}} \equiv 1/{}_jr_k^{\text{rel}}$ of the weighting matrix $W_k^{\text{rel}} \equiv (R_k^{\text{rel}})^{-1}$ tends to zero as ${}_j\Pi_k$ approaches unity. Similarly, the relative weight ${}_jw_k^{\text{rel}}$ is set to the maximum value of one for ${}_j\Pi_k = 0$. Consequently, a gradually degrading sensor carries monotonically decreasing weight in the computation of the estimate $\hat{\boldsymbol{x}}_k$ in Equation (20.12).

Next we set the bounds on the states ${}_j\Psi_k$ of the recursive relation in Equation (20.15). The lower limit of ${}_j\Pi_k$ (which is an algebraic function of ${}_j\Psi_k$) is set to the probability ${}_jp$ of intra-sample failure. On the other extreme, if ${}_j\Pi_k$ approaches unity, then the weight ${}_jw_k^{\text{rel}}$ (which approaches zero) may prevent fast restoration of a degraded sensor following its recovery. Therefore, the upper limit of ${}_j\Pi_k$ is set to $(1 - {}_j\alpha)$, where ${}_j\alpha$ is the allowable probability of false alarms of the jth measurement. Consequently, the function $h(\cdot)$ in Equation (20.17) is restricted to the domain $[{}_jp, (1 - {}_j\alpha)]$ to account for probabilities of intra-sampling failures and false alarms. Following Equation (20.15), the lower and

upper limits of the states ${}_j\Psi_k$ are thus become ${}_jp/(1-{}_jp)$ and $(1-{}_j\alpha)/{}_j\alpha$ respectively. Consequently, the initial state in Equation (20.15) is set as ${}_j\Psi_0 = {}_jp/(1-{}_jp)$ for $j = 1, 2, \ldots, \ell$.

20.2.2 Possible Modifications of the Calibration Filter

The calibration filter is designed to operate in conjunction with an FDI system that is capable of detecting and isolating abrupt disruptions (in excess of specified bounds) in one or more of the redundant measurements [7]. The consistent measurements, identified by the FDI system, are simultaneously calibrated at each sample. Therefore, if a continuous degradation, such as a gradual monotonic drift of a sensor amplifier, occurs sufficiently slowly relative to the filter dynamics, then the remaining (healthy) measurements might be affected, albeit by a small amount, due to simultaneous calibration of all measurements, including the degraded measurement. Thus, the fault may be disguised in the sense that a very gradual degradation over a long period may potentially cause the estimate $\hat{\boldsymbol{x}}_k$ to drift. This problem could be resolved by modifying the calibration filter with one or both of the following procedures:

- *Adjustments via limit check on the correction vector* $\hat{c}_k$. Compensation of a (slowly varying) undetected error in the jth measurement out of ℓ redundant measurements will cause the largest jth element $\left|{}_j\hat{c}_k\right|$ in the correction vector $\hat{c}_k$. Therefore, a limit check on the magnitude of each element of $\hat{c}_k$ will allow detection and isolation of the degraded measurement. The bounds of limit check, which could be different for the individual elements of $\hat{c}_k$, are selected by trade-off between the probability of false alarms and the allowable error in the estimate $\hat{\boldsymbol{x}}_k$ of the measured variable [12].
- *Usage of additional analytical measurements*. If the estimate $\hat{\boldsymbol{x}}_k$ is used to generate an analytic measurement of another plant variable that is directly measured by its own sensor(s), then a possible drift of the calibration filter can be detected whenever this analytical measurement disagrees with the sensor data in excess of a specified bound. The implication is that either the analytical measurement or the sensor is faulty. Upon detecting such a fault, the actual cause needs to be identified based on additional information, including reasonability check. This procedure not only checks the calibration filter but also guards against simultaneous and identical failure of several sensors in the redundant set, possibly due to a common cause, known as the common-mode fault.

20.3 Sensor Calibration in a Commercial-Scale Fossil-Fuel Power Plant

The calibration filter, derived above, has been validated in a 320 MWe coal-fired supercritical power plant for on-line sensor calibration and measurement estimation at the throttle steam condition of ~1040°F (560°C) and ~3625 psia (25.0 MPa). The set of redundant measurements is generated by four temperature sensors installed at different spatial locations of the main steam header that carries superheated steam from the steam generator into the high-pressure turbine via the throttle valves and governor valves [13]. Since these sensors are not spatially collocated, they can be asynchronous under transient conditions due to the transport lag. The filter simultaneously calibrates the sensors to generate a time-dependent estimate of the throttle steam temperature that is spatially averaged over the main steam header. This information on the estimated average temperature is used for health monitoring and damage prediction in the main steam header, as well as for coordinated feedforward–feedback control of the power plant under both steady-state and transient operations [14,15]. The filter software is hosted in a Pentium platform.

The readings of all four temperature sensors have been collected over a period of 100 h at a sampling frequency of once every 1 min. The data collected, after bad-data suppression (e.g. elimination of obvious outliers following built-in tests, such as limit check and rate check), show that each sensor

exhibits temperature fluctuations resulting from the inherent thermal–hydraulic noise and process transients, as well as the instrumentation noise. For this specific application, the parameters, functions, and matrices of the calibration filter are selected as described below.

20.3.1 Filter Parameters and Functions

We start with the filter parameters and functions that are necessary for degradation monitoring. In this application, each element of the residual vector η_k of the calibrated measurement vector y_k is assumed to be Gaussian distributed that assures existence of the likelihood ratios in Equation (20.15). The structures of the *a priori* conditional density functions are chosen as follows:

$$\begin{aligned} {}_jf^0(\varphi) &= \frac{1}{\sqrt{2\pi}\,{}_j\sigma}\exp\left(-\tfrac{1}{2}\left(\frac{\varphi}{{}_j\sigma}\right)^2\right) \\ {}_jf^1(\varphi) &= \frac{1}{\sqrt{2\pi}\,{}_j\sigma}\exp\left(-\tfrac{1}{2}\left(\frac{\varphi-{}_j\theta}{{}_j\sigma}\right)^2\right) \\ {}_jf^2(\varphi) &= \frac{1}{\sqrt{2\pi}\,{}_j\sigma}\exp\left(-\tfrac{1}{2}\left(\frac{\varphi+{}_j\theta}{{}_j\sigma}\right)^2\right) \end{aligned} \tag{20.18}$$

where ${}_j\sigma$ is the standard deviation, and ${}_j\theta$ and $-{}_j\theta$ are the thresholds for positive and negative failures respectively of the jth residual.

Since it is more convenient to work in the natural-log scale for Gaussian distribution than for the linear scale, an alternative to Equation (20.17) is to construct a monotonically decreasing continuous function g: $(-\infty, 0) \to (0, 1]$ in lieu of the monotonically increasing continuous function h: $[0, 1) \to [1, \infty)$, so that

$$W_{k+1}^{\text{rel}} \equiv \left(R_{k+1}^{\text{rel}}\right)^{-1} = \text{diag}\left[g\left(\ln {}_j\Pi_k\right)\right], \text{ i.e. the weight } {}_jw_{k+1}^{\text{rel}} \equiv \left({}_jr_{k+1}^{\text{rel}}\right)^{-1} = g\left(\ln {}_j\Pi_k\right) \tag{20.19}$$

The linear structure of the continuous function $g(\cdot)$ is chosen to be piecewise linear, as given below:

$$g(\varphi) = \begin{cases} w^{\max} & \text{for } \varphi \le \varphi^{\min} \\ \dfrac{(\varphi^{\max}-\varphi)w^{\max} + (\varphi-\varphi^{\min})w^{\min}}{\varphi^{\max}-\varphi^{\min}} & \text{for } -\infty \le \varphi^{\min} \le \varphi \le \varphi^{\max} < 0 \\ w^{\min} & \text{for } \varphi \ge \varphi^{\max} \end{cases} \tag{20.20}$$

The function $g(\cdot)$ maps the space of ${}_j\Pi_k$ in the log scale into the space of the relative weight ${}_jw_{k+1}^{\text{rel}}$ of individual sensor data. The domain of $g(\cdot)$ is restricted to $[\ln({}_jp), \ln(1-{}_j\alpha)]$ to account for probability ${}_jp$ of intra-sampling failure and probability ${}_j\alpha$ of false alarms for each of the four sensors. The range of $g(\cdot)$ is selected to be $[{}_jw^{\min}, 1]$ where a positive minimum weight (i.e. ${}_jw^{\min} > 0$) allows the filter to restore a degraded sensor following its recovery. Numerical values of the filter parameters ${}_j\sigma$, ${}_j\theta$, ${}_jp$, ${}_j\alpha$, and ${}_jw^{\min}$ are presented below:

- The standard deviations of the *a priori* Gaussian density functions of the four temperature sensors are:
  ${}_1\sigma = 4.1^\circ\text{F}(2.28^\circ\text{C})$; ${}_2\sigma = 3.0^\circ\text{F}(1.67^\circ\text{C})$; ${}_3\sigma = 2.4^\circ\text{F}(1.33^\circ\text{C})$; ${}_4\sigma = 2.8^\circ\text{F}(1.56^\circ\text{C})$

The initial condition for the measurement noise covariance matrix is set as $R_0 = \text{diag}[{}_j\sigma]$. The failure threshold parameters are selected as: ${}_j\theta = {}_j\sigma/2$ for $j = 1, 2, 3, 4$.

- The probability of intra-sampling failure is assumed to be identical for all four sensors, as they are similar in construction and operate under an identical environment. Operation experience at the power plant shows that the mean life of a resistance thermometer sensor, installed on the mean steam header, is about 700 days (i.e. about 2 years) of continuous operation. For a sampling interval of 1 min, this information leads to AO2

  $$_jp \approx 10^{-6} \quad \text{for } j = 1, 2, 3, 4$$

- The probability of false alarms is selected in consultation with the plant operating personnel. On average, each sensor is expected to generate a false alarm after approximately 700 days of continuous operation (i.e. once in 2 years). For a sampling interval of 1 min, this information leads to

  $$_j\alpha \approx 10^{-6} \quad \text{for } j = 1, 2, 3, 4$$

- To allow restoration of a degraded sensor following its recovery, the minimum weight is set as

  $$_jw_{\min} \approx 10^{-3} \quad \text{for } j = 1, 2, 3, 4$$

20.3.2 Filter Matrices

After conversion of the four temperature sensor data into engineering units, the scale factor matrix in Equation (1) becomes: $H = \begin{bmatrix} 1 & 1 & 1 & 1 \end{bmatrix}^{\mathrm{T}}$. Consequently, following Potter and Suman and Ray and Luck (1991), the parity space projection matrix in Equation (20.6) becomes

$$V = \begin{bmatrix} \sqrt{\frac{3}{4}} & -\sqrt{\frac{1}{12}} & -\sqrt{\frac{1}{12}} & -\sqrt{\frac{1}{12}} \\ 0 & \sqrt{\frac{2}{3}} & -\sqrt{\frac{1}{6}} & -\sqrt{\frac{1}{6}} \\ 0 & 0 & \sqrt{\frac{1}{2}} & -\sqrt{\frac{1}{2}} \end{bmatrix}$$

In the event of a sensor being isolated as faulty, sensor redundancy reduces to three, for which

$$H = \begin{bmatrix} 1 & 1 & 1 \end{bmatrix}^{\mathrm{T}} \quad \text{and} \quad V = \begin{bmatrix} \sqrt{\frac{2}{3}} & -\sqrt{\frac{1}{6}} & -\sqrt{\frac{1}{6}} \\ 0 & \sqrt{\frac{1}{2}} & -\sqrt{\frac{1}{2}} \end{bmatrix}$$

The ratio, $R_k^{-1/2} Q R_k^{-1/2}$, of covariance matrices Q and R_k in Equations (20.4) and (20.1) largely determines the characteristics of the minimum variance filter in Equation (20.8) or Equation (20.11). AQ3 The filter gain Γ_k increases with a larger ratio $R_k^{-1/2} Q R_k^{-1/2}$ and *vice versa*. Since the initial steady-state value R_0 is specified and R_k^{rel} is recursively generated thereon to calculate R_k via Equation (20.16), the choice is left only for selection of Q. As *a priori* information on Q may not be available, its choice relative to R_0 is a design feature. In this application, we have set $Q = R_0$.

20.3.3 Filter Performance Based on Experimental Data

The filter was tested on-line in the power plant over a continuous period of 9 months except for two short breaks during plant shutdown. The test results showed that the filter was able to calibrate each

sensor under both pseudo-steady-state and transient conditions under closed-loop control of throttle steam temperature. The calibrated estimate of the throttle steam temperature was used for plant control under steady-state, load-following, start-up, and scheduled shutdown conditions. No natural failure of the sensors occurred during the test period, and there was no evidence of any drift of the estimated temperature. As such, the modifications (e.g. adjustments via limit check on $\hat{c}_k$, and additional analytical measurements) of the calibration filter, described earlier in this chapter, were not implemented. In addition to testing under on-line plant operation, simulated faults have been injected into the plant data to evaluate the efficacy of the calibration filter under sensor failure conditions. Based on the data of four temperature sensors that were collected at an interval of 1 min over a period of 0 to 100 h, the following three cases of simulated sensor degradation are presented below:

20.3.3.1 Case 1 (Drift Error and Recovery in a Single Sensor)

Starting at 12.5 h, a drift error was injected into the data stream of Sensor#1 in the form of an additive ramp at the rate of 1.167°F (0.648°C) per hour. The injected fault was brought to zero at 75 h, signifying that the faulty amplifier in the sensor hardware was corrected and reset.

The simulation results in Figure 20.1 exhibit how the calibration filter responds to a gradual drift in one of the four sensors while the remaining three are normally functioning. Figure 20.1(a) shows the response of the four uncalibrated sensors and the estimate generated by simple averaging (i.e. fixed identical weights) of these four sensor readings at each sample. The sensor data profile includes transients lasting from ~63 to ~68 h. From time 0 to 12.5 h, when no fault is injected, all sensor readings are clustered together. Therefore, the uncalibrated estimate, shown by a thick solid line, is in close agreement with all four sensors during the period 0 to 12.5 h. Sensor#1, shown by the dotted line, starts drifting at 12.5 h while the remaining sensors stay healthy. Consequently, the uncalibrated estimate starts drifting at one quarter of the drift rate of Sensor#1 because of equal weighting of all sensors in the absence of the calibration filter. Upon termination of the drift fault at 75 h, when Sensor#1 is brought back to the normal state, the uncalibrated estimate resumes its normal state close to all four sensors for the remaining period from 75 to 100 h.

In Figure 20.1(b) shows the response of the four calibrated sensors and the estimate generated by weighted averaging (i.e. varying nonidentical weights) of these four sensor readings at each sample. The calibrated estimate in (b) stays with the remaining three healthy sensors even though Sensor#1 is gradually drifting. Figure 20.1(f) shows that, after the fault injection, Sensor#1 is weighted less than the remaining sensors. This is due to the fact that the residual η_k^1 [see Equation (20.13)] of Sensor#1 in Figure 20.1(c) increases in magnitude with the drift error. The profile of ${}_1w^{\text{rel}}$ in Figure 20.1(f) is governed by its nonlinear relationship with η_k^1 given by Equations (20.15), (20.19) and (20.20). As seen in Figure 20.1(f), ${}_1w^{\text{rel}}$ initially changes very slowly to ensure that it is not sensitive to small fluctuations in sensor data due to spurious noise, such as that resulting from thermal–hydraulic turbulence. The significant reduction in ${}_1w^{\text{rel}}$ takes place after about 32 h and eventually reaches the minimum value of 10^{-3} when η_k^1 is sufficiently large. Therefore, the calibrated estimate $\hat{\boldsymbol{x}}_k$ is practically unaffected by the drifting sensor and stays close to the remaining three healthy sensors. In essence, $\hat{\boldsymbol{x}}_k$ is the average of the three healthy sensors. Upon restoration of Sensor#1 to the normal state, the calibrated signal ${}_1y_k$ temporarily goes down because of the large value of correction ${}_1\hat{c}_k$ at that instant as seen in Figure 20.1(e). However, the adaptive filter quickly brings back ${}_1\hat{c}_k$ to a small value, and thereby the residual ${}_1\eta_k$ is reduced and the original weight (i.e. ~1) is regained. Calibrated and uncalibrated estimates are compared in Figure 20.1(d), which shows a peak difference of about 12°F (6.67°C) over a prolonged period.

In addition to the accuracy of the calibrated estimate, the filter provides fast and smooth recovery from abnormal conditions under both steady-state and transient operations of the power plant. For example, during the transient disturbance after about 65 h, the steam temperature undergoes a relatively large swing. Since the sensors are not spatially collocated, their readings are different during plant transients as a result of transport lag in the steam header. Figure 20.1(f) shows that the weights of two sensors out of the three healthy sensors are temporarily reduced while the remaining healthy sensor

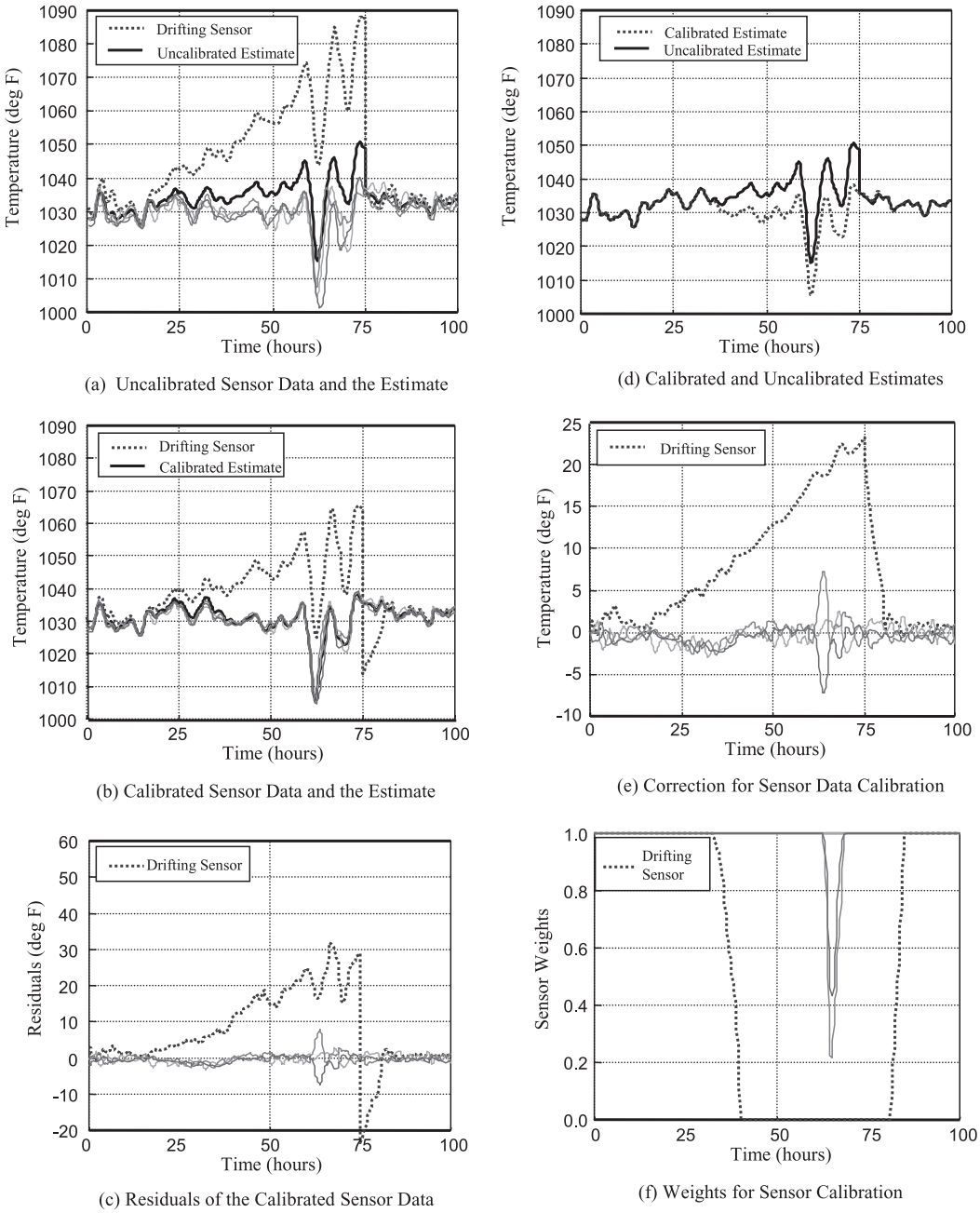

Figure 20.1. Performance of the calibration filter for drift error in a sensor.

enjoys the full weight and the drifting Sensor#1 has practically no weight. As the transients are over, three healthy sensors resume the full weight. The cause of weight reduction is the relatively large residuals of these two sensors, as seen in Figure 20.1(c). During this period, the two affected sensors undergo modest corrections: one is positive and the other negative, as seen in Figure 20.1(e), so that the calibrated values of the three healthy sensors are clustered together. The health-monitoring system and the plant control system rely on the spatially averaged throttle steam temperature [14–17].

Another important feature of the calibration filter is that it reduces the deviation of the drifting Sensor#1 from the remaining sensors as seen from a comparison of its responses in

Figure 20.1(a) and (b). This is very important from the perspectives of fault detection and isolation for the following reason. In an uncalibrated system, Sensor#1 might have been isolated as faulty due to accumulation of the drift error. In contrast, the calibrated system makes Sensor#1 temporarily ineffective without eliminating it as faulty. A warning signal can easily be generated when the weight of Sensor#1 diminishes to a small value. This action will draw the attention of maintenance personnel for possible repair or adjustment. Since the estimate $\hat{x}_k$ is not poisoned by the degraded sensor, a larger detection delay can be tolerated. Consequently, the allowable threshold for fault detection can be safely increased to reduce the probability of false alarms.

20.3.3.2 Case 2 (Zero-Mean Fluctuating Error and Recovery in a Single Sensor)

We examine the filter performance by injecting a zero-mean fluctuating error to Sensor#3 starting at 12.5 h and ending at 75 h. The injected error is an additive sine wave of period ~36 h and amplitude 25°F (13.9°C). The simulation results in Figure 20.2 show how the calibration filter responds to the fluctuating error in Sensor#3 while the remaining three sensors (i.e. Sensor#1, Sensor#2 and Sensor#4) are functioning normally. To some extent, the filter response is similar to that of the drift error in Case 1. The major difference is the oscillatory nature of the weights and corrections of Sensor#3, as seen in Figure20.2(f) and (e) respectively. Note that this simulated fault makes the filter switch autonomously to the normal state from either one of the two abnormal states as the sensor error fluctuates between positive and negative limits. Since this is a violation of the Assumption A3 in Appendix A, the recursive relation in Equation (20.A17) represents an approximation of the actual situation. The results in Figure 20.2(b) to (f) show that the filter is sufficiently robust to be able to execute the tasks of sensor calibration and measurement estimation in spite of this approximation. The filter not only exhibits fast response, but also its recovery is rapid regardless of whether the fault is naturally mitigated or corrected by an external agent.

20.3.3.3 Case 3 (Drift Error in One Sensor and Zero-Mean Fluctuating Error in Another Sensor)

This case investigates the filter performance in the presence of simultaneous faults in two out of four sensors. Note that if the two affected sensors have similar types of fault (e.g. common mode faults), the filter will require additional redundancy to augment the information base generated by the remaining healthy sensors. Therefore, we simulate simultaneous dissimilar faults by injecting a drift error in Sensor#1 and a fluctuating error in Sensor#3 exactly identical to those in Case 1 and Case 2 respectively. A comparison of the simulation results in Figure 20.3 with those in Figures 20.1 and 20.2 reveals that the estimate $\hat{x}_k$ is essentially similar in all three cases, except for small differences during the transients at ~65 h. It should be noted that, during the fault injection period from 12.5 to 75 h, $\hat{x}_k$ is strongly dependent on: Sensors#2, #3 and #4 in Case 1; Sensors#1, #2 and #4 in Case 2; and Sensors#2 and #4 in Case 3. Therefore, the estimate $\hat{x}_k$ cannot be exactly identical for these three cases. The important observation in this case study is that the filter can handle simultaneous faults in two out of four sensors provided that these faults are not strongly correlated; otherwise, additional redundancy or equivalent information would be necessary.

20.4 Summary and Conclusions

This chapter presents a formulation and validation of an adaptive filter for real-time calibration of redundant signals consisting of sensor data and/or analytically derived measurements. Individual signals are calibrated on-line by an additive correction that is generated by a recursive filter. The covariance matrix of the measurement noise is adjusted as a function of the *a posteriori* probabilities of failure of the individual measurements. An estimate of the measured variable is also obtained in real time as a weighted average of the calibrated measurements. These weights are recursively updated in real time instead of being fixed *a priori*. The effects of intra-sample failure and probability of false alarms are

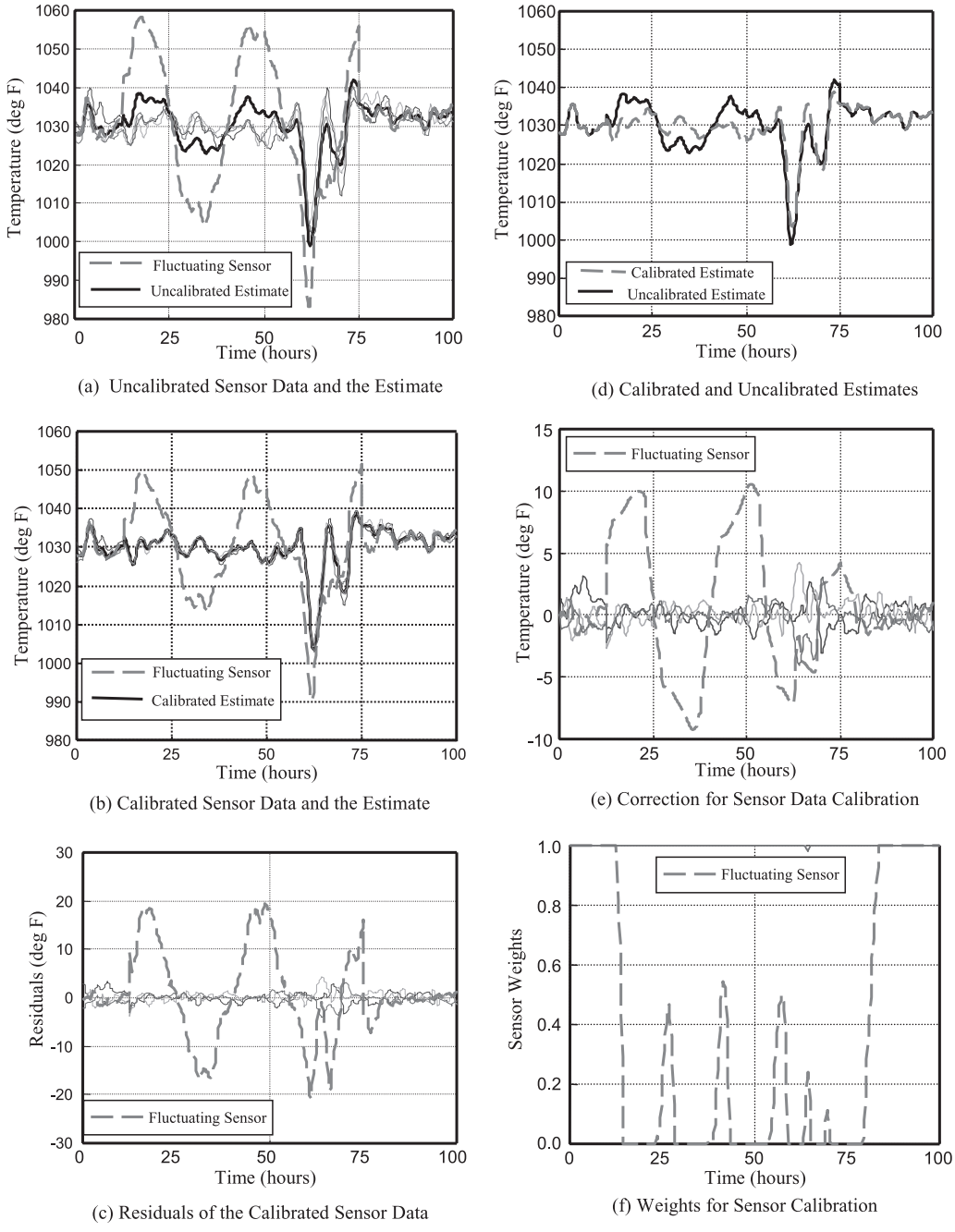

(a) Uncalibrated Sensor Data and the Estimate

(b) Calibrated Sensor Data and the Estimate

(c) Residuals of the Calibrated Sensor Data

(d) Calibrated and Uncalibrated Estimates

(e) Correction for Sensor Data Calibration

(f) Weights for Sensor Calibration

Figure 20.2. Performance of the calibration filter for fluctuation error in a sensor.

taken into account in the recursive filter. The important features of this real-time adaptive filter are summarized below:

- A model of the physical process is not necessary for calibration and estimation if sufficient redundancy of sensor data and/or analytical measurements is available.
- The calibration algorithm can be executed in conjunction with a fault-detection and isolation system.

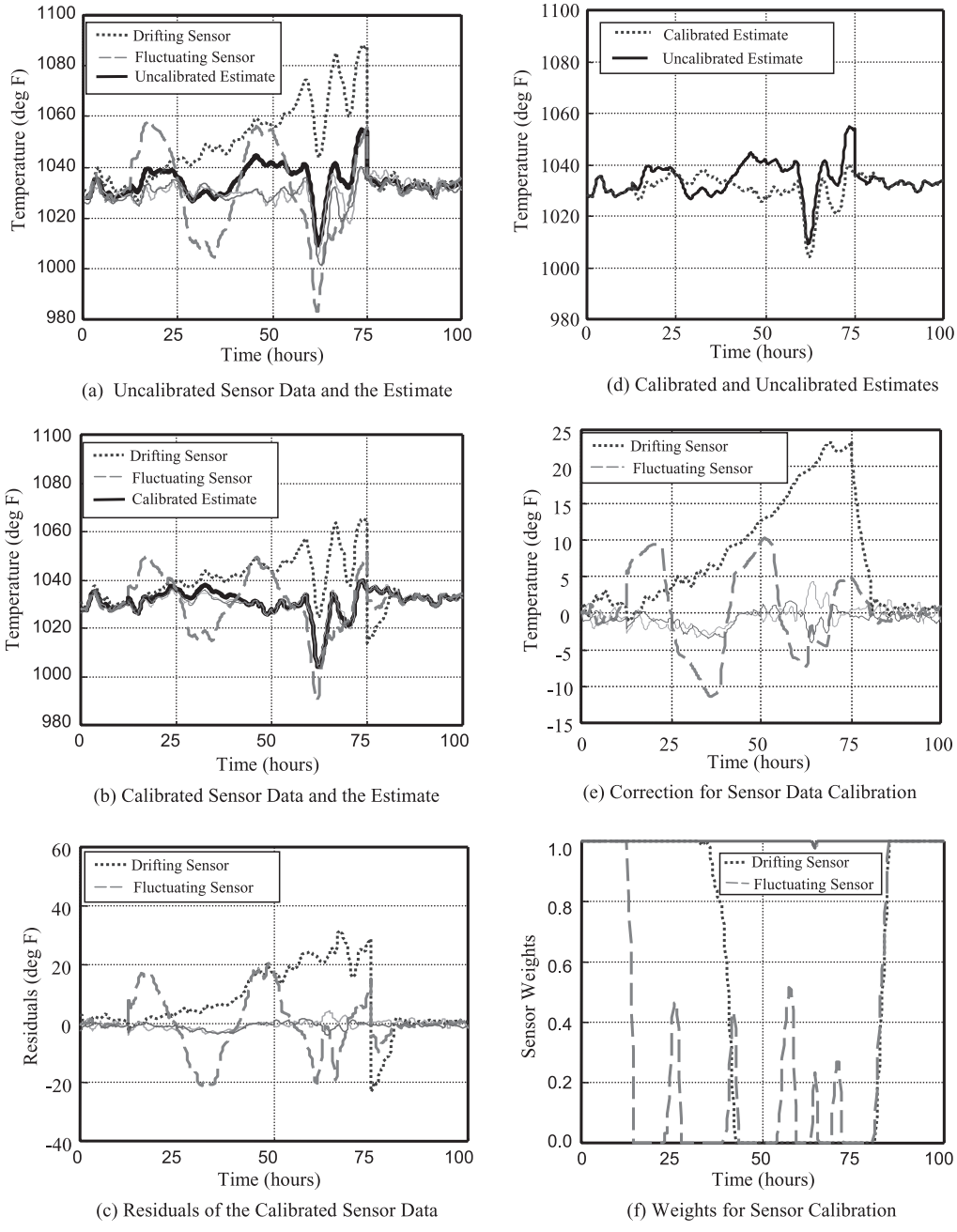

Figure 20.3. Performance of the calibration filter for drift error and fluctuation error in two sensors.

- The filter smoothly calibrates each measurement as a function of its *a posteriori* probability of failure, which is recursively generated based on the current and past observations.

The calibration and estimation filter has been tested by injecting faults in the data set collected from an operating power plant. The filter exhibits speed and accuracy during steady-state and transient operations of the power plant. It also shows fast recovery when the fault is corrected or naturally mitigated. The filter software is portable to any commercial platform and can be potentially used to

enhance the Instrumentation & Control System Software in tactical and transport aircraft, and nuclear and fossil-fuel power plants.

Appendix A: Multiple Hypotheses Testing Based on Observations of a Single Variable

Let $\{\eta_k, k = 1, 2, 3, \cdots\}$ be (conditionally) independent values of a single variable (e.g. residual of a measurement) at consecutive sampling instants. We assume M distinct possible modes of failure in addition to the normal mode of operation that is designated as the mode 0. Thus, there are $(M+1)$ mutually exclusive and exhaustive hypotheses defined at the kth sample as

$$\begin{aligned} &H_k^0\text{: } \textit{Normal behavior with} \text{ a priori } \textit{density function } f^0(\cdot) \equiv f\left(\cdot\middle|H^0\right) \\ &H_k^i\text{: } \textit{Abnormal behavior with} \text{ a priori } \textit{density function } f^i(\cdot) \equiv f\left(\cdot\middle|H^i\right),\ i = 1, 2, \ldots, M \end{aligned} \tag{20.A1}$$

where each hypothesis $H_k^j, j = 0, 1, 2, \ldots, M$ is treated as a Markov state.

We define the *a posteriori* probability π_k^j of the jth hypothesis at the kth sample as

$$\pi_k^j \equiv P[H_k^j|Z_k], j = 0, 1, 2, \ldots, M \tag{20.A2}$$

based on the history $Z_k \equiv \cap_{i=1}^k z_i$ where $z_i \equiv \{\eta_i \in B_i\}$ and B_i is the region of interest at the ith sample. The problem is to derive a recursive relation for *a posteriori* probability of failure Π_k at the kth sample:

$$\Pi_k \equiv P\left[\bigcup_{j=1}^M H_k^j|Z_k\right] = \sum_{j=1}^M P\left[H_k^j|Z_k\right] \Rightarrow \Pi_k = \sum_{j=1}^M \pi_k^j \tag{20.A3}$$

because of the exhaustive and mutually exclusive properties of the Markov states, $H_k^j, j = 1, 2, \ldots, M$. To construct a recursive relation for Π_k, we introduce the following three definitions:

$$\text{Joint probability: } \xi_k^j \equiv P[H_k^j, Z_k] \tag{20.A4}$$

$$A \textit{ priori} \text{ probability: } \lambda_k^j \equiv P[z_k|H_k^j.] \tag{20.A5}$$

$$\text{Transition probability: } \alpha_k^{i,j} \equiv P[H_k^j|H_{k-1}^i] \tag{20.A6}$$

Then, because of conditional independence of z_k and Z_{k-1}, Equation (A-4) takes the following form:

$$\begin{aligned} \xi_k^j &= P[H_k^j, z_k, Z_{k-1}] \\ &= P[z_k\left|H_k^j\right]P[H_k^j, Z_{k-1}] \end{aligned} \tag{20.A7}$$

Furthermore, the exhaustive and mutually exclusive properties of the Markov states $H_k^j, j = 0, 1, 2, \ldots, M$, and independence of Z_{k-1} and H_k^j lead to

$$\begin{aligned} P\left[H_k^j, Z_{k-1}\right] &= \sum_{i=0}^M P\left[H_k^j, H_{k-1}^i, Z_{k-1}\right] \\ &= \sum_{i=0}^M P\left[Z_{k-1}\middle|H_{k-1}^i\right]P\left[H_k^j\middle|H_{k-1}^i\right]P\left[H_{k-1}^i\right] \\ &= \sum_{i=0}^M P\left[H_k^j\middle|H_{k-1}^i\right]P\left[H_{k-1}^i, Z_{k-1}\right] \end{aligned} \tag{20.A8}$$

The following recursive relation is obtained from a combination of Equations (20.A4) to (20.A8) as:

$$\xi_k^j = \lambda_k^j \sum_{i=0}^{M} a_k^{i,j} \xi_{k-1}^i \tag{20.A9}$$

We introduce a new term

$$\psi_k^j \equiv \frac{\xi_k^j}{\xi_k^0} \tag{20.A10}$$

that reduces to the following form by use of Equation (20.A9):

$$\psi_k^j = \left(\frac{\lambda_k^j}{\lambda_k^0}\right)\left(\frac{a_k^{0,j} + \sum_{i=1}^{M} a_k^{i,j}\psi_{k-1}^i}{a_k^{0,0} + \sum_{i=1}^{M} a_k^{i,0}\psi_{k-1}^i}\right) \tag{20.A11}$$

to obtain the *a posteriori* probability π_k^j in Equation (20.A2) in terms of ξ_k^j and ψ_k^j as

$$\begin{aligned}\pi_k^j &= \frac{P[H_k^j, Z_k]}{P[Z_k]} = \frac{P[H_k^j, Z_k]}{\sum_{i=0}^{M} P\left[H_k^i, Z_k\right]} \\ &= \frac{\xi_k^j}{\xi_k^0 + \sum_{i=1}^{M} \xi_k^i} = \frac{\psi_k^j}{1 + \sum_{i=1}^{M} \psi_k^i}\end{aligned} \tag{20.A12}$$

A combination of Equations (20.A3) and (20.A12) leads to the *a posteriori* probability Π_k of failure as

$$\Pi_k = \frac{\Psi_k}{1 + \Psi_k} \quad \text{with} \quad \Psi_k \equiv \sum_{j=1}^{M} \psi_k^j \tag{20.A13}$$

The above expressions can be realized by a simple recurrence relation under the following four assumptions:

- *Assumption A1.* At the starting point (i.e. $k = 0$), all measurements operate in the normal mode, i.e. $P[H_0^0] = 1$ and $P[H_0^j] = 0$ for $j = 1, 2, \ldots, M$. Therefore, $\xi_0^0 = 1$ and $\xi_0^j = 0$ for $j = 1, 2, \ldots, M$.
- *Assumption A2.* Transition from the normal mode to any abnormal mode is equally likely. That is, if p is the *a priori* probability of failure during one sampling interval, then $a_k^{0,0} = 1 - p$ and $a_k^{0,i} = p/M$ for $i = 1, 2, \ldots, M$, and all k.
- *Assumption A3.* No transition takes place from an abnormal mode to the normal mode, implying that $a_k^{i,0} = 0$ for $i = 1, 2, \ldots, M$, and all k. The implication is that a failed sensor does not return to the normal mode (unless replaced or repaired).
- *Assumption A4.* Transition from an abnormal mode to any abnormal mode, including itself, is equally likely. That is, $a_k^{i,j} = 1/M$ for $i, j = 1, 2, \ldots, M$, and all k.

A recursive relation for Ψ_k is generated based on the above assumptions and using the expression in Equation (20.A11) as

$$\psi_k^j = \frac{p + \sum_{i=1}^{M} \psi_{k-1}^i}{(1-p)M} \left(\frac{\lambda_k^j}{\lambda_k^0} \right) \quad \text{given} \quad \psi_0^j = 0 \quad \text{for} \quad j = 1, 2, \ldots, M \tag{20.A14}$$

which is simplified by use of the relation $\Psi_k \equiv \sum_{i=1}^{M} \psi_k^i$ in Equation (20.A13) as

$$\Psi_k = \left(\frac{p + \Psi_{k-1}}{(1-p)M} \right) \sum_{j=1}^{M} \frac{\lambda_k^j}{\lambda_k^0} \quad \text{given} \quad \Psi_0 = 0 \tag{20.A15}$$

If the probability measure associated with each abnormal mode is absolutely continuous relative to that associated with the normal mode, then the ratio λ_k^j/λ_k^0 of *a priori* probabilities converges to a Radon–Nikodym derivative as the region B_k in the expression $z_k \equiv \{\eta_k \in B_k\}$ approaches zero measure [18]. This Radon–Nikodym derivative is simply the likelihood ratio $f^j(\eta_k)/f^0(\eta_k), j = 1, 2, \ldots, M,$ where $f^i(\cdot)$ is the *a priori* density function conditioned on the hypothesis H^i, $i = 0, 1, 2, \ldots, M$.

Accordingly, Equation (20.A15) becomes

$$\Psi_k = \left(\frac{p + \Psi_{k-1}}{(1-p)M} \right) \sum_{j=1}^{M} \frac{f^j(\eta_k)}{f^0(\eta_k)} \quad \text{given} \quad \Psi_0 = 0 \tag{20.A16}$$

For the specific case of two abnormal hypotheses (i.e. $M = 2$) representing positive and negative failures, the recursive relations for Ψ_k and Π_k in Equations (20.A16) and (20.A13) become

$$\left.\begin{aligned} \Psi_k &= \left(\frac{p + \Psi_{k-1}}{2(1-p)} \right) \left(\frac{f^1(\eta_k) + f^2(\eta_k)}{f^0(\eta_k)} \right) \\ \Pi_k &= \frac{\Psi_k}{1 + \Psi_k} \end{aligned}\right\} \quad \text{given} \quad \Psi_0 = 0 \tag{20.A17}$$

References

[1] Dickson, B. *et al.*, Usage and structural life monitoring with HUMS, in *American Helicopter Society 52nd Annual Forum*, Washington, DC, June 4–6, 1996, 1377.

[2] Potter, J.E. and Suman, M.C., Thresholdless redundancy management with arrays of skewed instruments, in Integrity in Electronic Flight Control Systems, NATO AGARDOGRAPH-224, 1977, 15-1.

[3] Daly, K.C. *et al.*, Generalized likelihood test for FDI in redundant sensor configurations, *Journal of Guidance and Control*, 2(1), 9, 1979.

[4] Ray, A. *et al.*, Analytic redundancy for on-line fault diagnosis in a nuclear reactor, *AIAA Journal of Energy*, 7(4), 367, 1983.

[5] Deckert, J.C. *et al.*, Signal validation for nuclear power plants, *ASME Journal of Dynamic Systems, Measurement and Control*, 105(1), 24, 1983.

[6] Desai, M.N. *et al.*, Dual sensor identification using analytic redundancy, *Journal of Guidance and Control*, 2(3), 213, 1979.

[7] Ray, A. and Desai, M., A redundancy management procedure for fault detection and isolation, *ASME Journal of Dynamic Systems, Measurement and Control*, 108(3), 248, 1986.

AQ4

[8] Ray, A. and Phoha, 2002.
[9] Ray, A. and Luck, R., Signal validation in multiply-redundant systems, *IEEE Control Systems Magazine*, 11(2), 44, 1996.
[10] Jazwinski, A.H., *Stochastic Processes and Filtering Theory*, Academic Press, New York, 1970.
[11] Gelb, A. (ed.), *Applied Optimal Estimation*, MIT Press, Cambridge, MA, 1974.
[12] Ray, A., Sequential testing for fault detection in multiply-redundant systems, *ASME Journal of Dynamic Systems, Measurement and Control*, 111(2), 329, 1989.
[13] Stultz, S.C. and Kitto, J.B. (eds), *Steam: Its Generation and Use*, 40th ed., Babcock & Wilcox Co., Baberton, OH, 1992.
[14] Kallappa, P.T. *et al*., Life extending control of fossil power plants for structural durability and high performance, *Automatica*, 33(6), 1101, 1997.
[15] Kallappa, P.T. and Ray, A., Fuzzy wide-range control of fossil power plants for life extension and robust performance, *Automatica*, 36(1), 69, 2000.
[16] Holmes, M. and Ray, A., Fuzzy damage mitigating control of mechanical structures, *ASME Journal of Dynamic Systems, Measurement and Control*, 120(2), 249, 1998.
[17] Holmes, M. and Ray, A., Fuzzy damage mitigating control of a fossil power plant, *IEEE Transactions on Control Systems Technology*, 9(1), 140, 2001.
[18] Wong, E. and Hajek, B., *Stochastic Processes in Engineering Systems*, Springer-Verlag, New York, 1985.